DOI: 10.13009/EUCASS2019-130

AERODATABASE OF VEGA-C LAUNCHER DEVELOPMENT AND INTEGRATION

Pietro Roncioni [(1)], Pier Luigi Vitagliano [(1)], Fabrizio De Gregorio [(1)], Fabio Paglia [(2)], Claudio Milana [(2)]
[(1)] CIRA, via Maiorise – 81043 Capua (CE), Italy
[(2)] AVIO Spa, via Ariana km 5,2 – 00034 Colleferro (Rome), Italy

Abstract

In the framework of VECEP Program (Vega Consolidation and Evolution Preparation) whose target is the development of the VEGA C Launcher, characterized by higher capabilities in terms of payloads and propulsion power, CIRA has been assigned by AVIO of the building of the aerodynamic database (ADB). This has been obtained by means of both wind tunnel tests and CFD simulations that coupled with suitable aerodynamic and uncertainties models gave the aerodynamic coefficients in the ranges of required Mach and attitude and along the given trajectory. In this paper the final aero-database and the whole building process are presented and comparisons between wind tunnel data and CFD simulations are shown.

1. Introduction

One of the main tasks within the framework of VECEP Program is the development of the launcher VEGA C aerodynamic database (ADB). The ADB, coupled with a suitable uncertainties model, is of paramount importance being the input for flight mechanics analysis and structural calculations; it has been obtained by means of both wind tunnel tests and numerical calculations.
Wind tunnel tests have been carried out in the critical transonic and low supersonic regimes at INCAS trisonic facility located in Bucharest (Romania). CFD simulations have been carried out at CIRA (the Italian Aerospace Research Centre) and cover all the Mach number range of the atmospheric flight, with the objective of generating the database in the hypersonic regime and supporting the extrapolation to flight of wind tunnel data in the other flow regimes.
The final ADB is a combination of experimental data and numerical results together with uncertainties values and dispersion errors in order to produce a confidence level model coupled to the nominal values of the aerodynamic coefficients.
A build-up approach has been used for both the nominal and the confidence level values, consisting in a linear summation of several contributions. Two regimes of Mach number have been considered depending on the availability or not of experimental data. In particular, in the sub-transonic regime, where experimental data are available, the main contribution to the aero-database comes from the wind tunnel measurements that are corrected and integrated with CFD simulations, while in the hypersonic regime the aerodynamic coefficients are obtained by means of dedicated numerical activities.

2. Program and Vehicle Description

The VEga Consolidation and Evolution Programme (VECEP) has entered into force on 21 November 2012, following subscriptions made by participating States at the occasion of the ESA Council meeting at ministerial level in Naples. Following the Scenarios Expert Group sessions hold during summer 2014, a new orientation in the Ariane programmes has been defined, which has impacted the Vega evolution scenario. Indeed, it has been decided to develop a common Solid Rocket Motor (SRM) (hereafter named P120C) to be used both as Vega 1st stage and strap-on boosters for the Ariane 6-2 (2 boosters) and Ariane 6-4 (4 boosters) configurations. Furthermore, this change on the 1st stage propulsion has led to suggest the substitution of the Zefiro 23 (Z23) with a new 2nd stage SRM - the Zefiro 40 (Z40) - which provides a better staging of the Vega launcher. The new baseline architecture for Vega C has become then: P120C/Z40/Z9/AVUM+, being the AVUM+ an upgrading of the VEGA four stage AVUM (Attitude and Vernier Upper Module) and Z9 the third stage Zefiro 9 solid rocket motor.
The VEGA C launcher is accordingly an evolution of the current Vega launcher. It will enable significant advances in terms of performance and costs: increasing of load capacity from the current 1,500 kg to 2,200 kg in Low Earth Orbit (700 km) and more competitive costs, thanks to the reorganization of production processes and a more efficient production chain. Main differences in the external shape are a larger payload fairing, the substitution of the first stage

DOI: 10.13009/EUCASS2019-130

P80 with the larger P120, a new second stage (Z40 in substitution of Z23), new larger interstages, larger number of retro rockets and non symmetric external fairing components. More specifically, the gain in performance – w.r.t the current Vega – shall at least balance/compensate the losses related to the applicable safety constrains (e.g. FSOA, Space Debris Policy) and provide additional margin for complex missions requiring significant flexibility in the flight strategy, without any increase of the recurring costs. Options to enlarge the potential market by providing cost efficient launch service solution will be studied in particular for new strategy to orbit, using electric propulsion for servicing Medium-Earth Orbit (MEO) or Geostationary Orbit GEO Small Satellite market, and new solutions for accommodation of small-sats, in a multiple launch configuration.

3. Aero Data Base Building

Two ranges of Mach are considered: M=0.5 – 3.5 (subsonic-transonic-supersonic) for which both WT and CFD data are available and M=3.5 – 7.0 (hypersonic) where only CFD data are used for building of the aerodatabase. This approach is due to the choice of focusing the experimental campaign, conducted at INCAS trisonic wind tunnel in Bucharest, on a limited range of Mach number with respect to the flight envelope. The results of previous VEGA test campaigns ([1], [2], [3]) are used in order to make up for this lack of data. Since separation occurs at about Mach=5.9 (time=140 s) the three stage configuration had to be simulated, in the hypersonic range, in addition to the four stage one (Figure 1).
The aero-database is obtained by means of a build-up approach used for both the coefficients and the uncertainties levels. The output of the aero data package is constituted by the six aerodynamic coefficients (global, lumped and distributed) and the pressure distribution: CL, CD, CS, CMx, CMy, CMz, p=p(surface). The independent variables are: Mach number, angle of attach α, Reynolds number Rey, roll angle ϕ.
Each aerodynamic contribution is a summation of several contributions and each of this contribution is function of one or more variables.
In particular, we have for each Mach range the following formulas:

Sub-transonic-supersonic range (M = 0.5 – 3.5)

$$C_{i,N}^{FL}(\alpha, M, Re, \varphi) =$$ **Nominal generic coefficient in flight cond.**

$$C_{i,WT}(\alpha, M) +$$ *WT clean contribution*

$$\Delta C_{i,WT}^{Prot}(\alpha, M, \varphi) +$$ *WT Protusion contribution*

$$\Delta C_{i,base}^{CFD}(\alpha, M, \varphi) +$$ *CFD Base contribution*

$$\Delta C_{i,Re}^{CFD}(\alpha, M, Re)$$ *CFD Re effect (Extrapolation to flight)*

Hypersonic range (M = 3-5 – 7.0)

$$C_{i,N}^{FL}(\alpha, M, Re, \varphi) =$$ **Nominal generic coefficient in flight cond.**

$$C_{i,CFD}(\alpha, M) +$$ *CFD Clean contribution*

$$\Delta C_{i,CFD}^{Prot}(\alpha, M, \varphi) +$$ *CFD Protusion contrribution*

The final Coefficient is the summation of the above nominal value and the uncertainty contribution:

$$C_{i}^{FL}(\alpha, M, Re, \varphi) =$$ **Generic coefficient in flight cond.**

$$C_{i,N}^{FL}(\alpha, M, Re, \varphi) +$$ Nominal generic coefficient in flight cond.

$$\Delta C_{i,UNC}(\alpha, M, Re, \varphi)$$ Uncertainty contribution

Where for sub-transonic-supersonic flow regimes we have:

$$\Delta C_{i,UNC}(\alpha, M, Re, \varphi) =$$

$$\Delta C_{i,UNC}^{WT}(\alpha, M, Re, \varphi) +$$ Wind Tunnel Uncertainty contribution

$$\Delta C_{i,UNC}^{CFD}(\alpha, M, Re, \varphi)$$ CFD-ETF Uncertainty contribution

DOI: 10.13009/EUCASS2019-130

And for hypersonic flow regime:

$$\Delta C_{i,UNC}(\alpha, M, Re, \varphi) =$$

$$\Delta C_{i,UNC}^{WTvsCFD}(\alpha, M, Re, \varphi) + \quad \text{Uncertainty due to unavailability of Exp data}$$

$$\Delta C_{i,UNC}^{CFD}(\alpha, M, Re, \varphi) \quad \text{CFD Uncertainty contribution}$$

The first term on the right hand side of the last formula (hypersonic regime) is taken into account instead of the wind tunnel uncertainty contribution. We took as a reference the differences between CFD and WT data from the VEGA 2003 campaign, assuming that they are comparable to the ones that we could have obtained today if we had performed experimental tests on VECEP in this Mach regime. Indeed the CFD code features are similar, as well as the launcher main characteristics, being the main difference the asymmetric layout of the protrusions.
A confidence level is required for each coefficient. This can be obtained adding to the uncertainty value, obtained as described above, the dispersion contribution. This last value takes into account the repeatability of experimental measurements and the non-perfect equivalence of models with the real world in terms of geometry and far-field conditions. This second contribution has to be taken into account for CFD modelling also because, as already said, the CAD model do not reproduce all the geometrical aspect and the far-field conditions of numerical simulation could differ from the real flight conditions.
In general, we can consider the following prospect:

Uncertainties:
- WT balance
- WT corrections
- CFD-GRID
- CFD-Modeling
- CFD-NoExp (unavailability of experimental data)

Dispersions:
- WT repeatability
- Difference of WT model and/or testing wrt flight conditions
- Difference of CFD model and/or running wrt flight conditions

The CFD-NoExp takes into account for the lack of experimental data in the hypersonic range and for some parts in the transonic range (no base drag measurements and no measurements with canted nozzle).
The difference of the models with the real world is taken into account by means of an increment of the basic uncertainties of a percentage in agreement with the client (5%).

4. Numerical activities

Several VEGA-C configurations have been taken into account for the development of the database. The main ones are: a four-stage clean one simulated in motor-on conditions at four different Reynolds number (two of them for comparison with WT tests, one at flight conditions and one intermediate between WT and flight) and two angles of attack in order to establish suitable laws for extrapolation to flight procedure. A second configuration (4-stage clean with sting) has been used for direct comparison of CFD results and WT measurements. The simulations of the 3-stage clean configuration were performed only at Reynolds flight conditions since in this regime we do not need extrapolation to flight.

4.1 CFD Methodology

The following CIRA in-house codes have been used, depending on the Mach regime.
For STS (SubTransSuper sonic) range, the code named ZEN (Zonal Euler Navier-stokes) has been adopted. ZEN is a multiblock structured flow solver for steady and unsteady Reynolds Averaged Navier Stokes (RANS) equations, which has been developed at CIRA for more than two decades [7], [8], [9], [13], [14], [15]. It is based upon cell centered, finite volumes formulation, with central schemes. Convergence toward steady state is achieved by explicit multi-stages Runge-Kutta schemes, with acceleration techniques like local time stepping, residual averaging and multigrid [10]. Several turbulence models are available; all solutions in the present work were computed using the k-ω TNT two equations model [12]. Condition of free transition from laminar to turbulent flow was selected. ZEN was used in the past for CFD analysis of VEGA configuration both in flight and in wind tunnel conditions ([1], [2]).
Comparisons with wind tunnel experiments carried out in the year 2004 on a 1:30 scaled model (3 stages and 4 stages configurations, with and without protrusions, including engine jet simulation) at FOI (Swedish Defense

DOI: 10.13009/EUCASS2019-130

Research Agency) and at DNW SST (German Dutch Wind Tunnel) and on two 1:40 scaled models at DLR Hypersonic facility H2K in Koeln, demonstrated good agreement in the complete range of Mach and Reynolds numbers considered.
For Hypersonic speed range, the NExT (Numerical Experimental Tool) code has been used ([16]). NExT solves, on a multi-block structured grid, the RANS equations in a density-based approach.
It allows the treatment of a wide range of compressible fluid dynamics problems for both aerothermodynamic and combustion applications. The Chemkin® input interface permits to treat different mixtures of reacting gases, specifying mixture composition and chemical kinetic scheme. A thermal database contains the transport coefficients and the thermodynamics data for each species.
Specific thermodynamics and transport models are available for aerothermodynamic applications.
The fluid can be treated as a mixture of gases in thermo-chemical non equilibrium. The energy exchange between vibrational and translational modes (TV) is modelled with the classical Landau-Teller non-equilibrium equation, with average relaxation times taken from the Millikan-White theory modified by Park. For what concerns transport coefficient, the species viscosity, and thermal conductivity, are calculated by means of the Eucken law whereas, the mixture viscosity and thermal conductivity are calculated by using the semi-empirical Wilke formulas. The diffusion coefficients are computed through a sum rule of the binary diffusivities for each couple of species. With respect to the numerical formulation, conservation equations are written in integral form, and discretized with a finite volume, cell centred, technique. Eulerian fluxes are computed with a Flux Difference Splitting (FDS) upwind method. Second order formulation is obtained by means of an Essentially Non Oscillatory (ENO) reconstruction of interface value. Viscous fluxes are computed with a classical centred scheme.
A two-equation k-ε turbulence modelling is used for eddy viscosity calculation while laminar-to-turbulence transition is imposed across surface lines (i.e. a transition front). Some versions of the two-equation k-ε model are available: standard, RNG and with compressibility effects correction for the present high speed turbulent flows simulations ([17]).

4.2 Numerical Results

The test matrix of all CFD simulations is reported in Table 1 and Table 2. The aim of the numerical simulations is both for extrapolations to flight of experimental measurements and for the building of a preliminary Aerodatabase based on CFD simulations only. Two configurations have been simulated, the 4-stage (Figure 1, above) flying up to about Mach 6 and the 3-stage (Figure 1, below) flying from Mach 6 to higher values. Mach 7 is the upper limit for the ADB. The 4-stage configuration has been simulated with two different nozzle positions: 0 and 6 degrees. In the range of Mach between 0.5 and 3.5 experimental data are available and so the CFD data are used for the extrapolation to flight and for estimation of the aerodynamic contributions not measured in wind tunnels (forces on base and nozzle). For higher Mach number, CFD simulations only are available to build the ADB. The reference quantities for the calculations of the aerodynamic conditions are the diameter of the first stage (L_{ref}) and the relevant surface (S_{ref}) and Moment Reference Centre is the launcher nose.

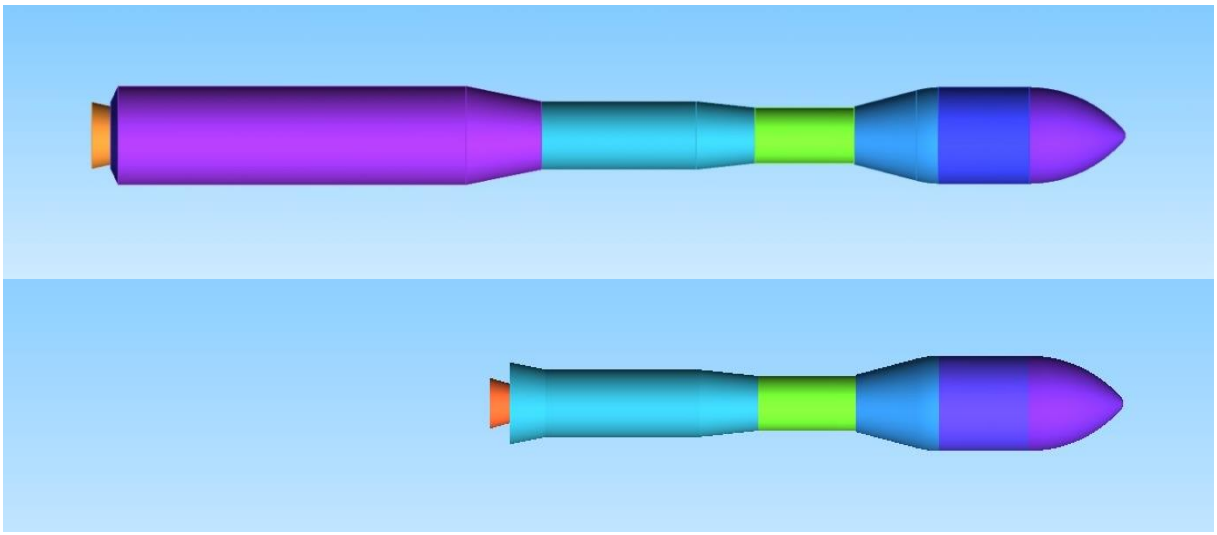

Figure 1: 4-stage and 3-stage version of VEGA C launcher. Clean configuration.

DOI: 10.13009/EUCASS2019-130

Table 1: CFD Test Matrix. 4 stage and 3 stage Baseline Configuration.

Regime	**Mach** [-]	**Reynolds** [-]	**AoA** [deg]	**Body grid**	**Conf.**	**Nozzle** [deg]
Sub-Transonic	0.50	WT, INT	5°	Half	baseline	0°
	0.50	Flight	0°,5°,10°	Half	baseline	0°
	0.80	Flight	0°,5°,10°	Half	baseline	0°
	0.85	Flight	0°,5°,10°	Half	baseline	0°
	0.95	WT, INT	5°	Half	baseline	0°
	0.95	Flight	0°,5°,10°	Half	baseline	0°
	1.05	WT, INT	5°	Half	baseline	0°
	1.05	Flight	0°,5°,10°	Half	baseline	0°
	1.10	Flight	0°,5°,10°	Half	baseline	0°
	1.20	WT, INT	5°	Half	baseline	0°
	1.20	Flight	0°,5°,10°	Half	baseline	0°
Supersonic	1.70	Flight	0°,5°,10°	Half	baseline	0°
	*1.70**	*Flight*	*0°,5°,10°*	*Half*	*baseline*	*6°*
	1.80	WT, INT	5°	Half	baseline	0°
	1.80	Flight	0°,5°,10°	Half	baseline	0°
	2.00	Flight	0°,5°,10°	Half	baseline	0°
	*2.00**	*Flight*	*0°,5°,10°*	*Half*	*baseline*	*6°*
	3.50	WT, INT	5°	Half	baseline	0°
	3.50	Flight	0°,5°,10°	Half	baseline	0°
Hypersonic 4S	5.00	Flight	0°,5°,10°	Half	baseline	0°
	5.44	Flight	0°,5°,10°	Half	baseline	0°
	5.91	Flight	0°,5°,10°	Half	baseline	0°
Hypersonic 3S	4.00	Flight	0°,5°,10°	Half	baseline	0°
	6.00	Flight	0°,5°,10°	Half	baseline	0°
	7.00	Flight	0°,5°,10°	Half	baseline	0°

Table 2: CFD Test Matrix. 4 stage Protrusion Configuration.

Regime	**Mach** [-]	**Reynolds** [-]	**AoA** [deg]	**roll** [deg]	**Body grid**	**Conf.**	**Nozzle** [deg]
Sub-Transonic	0.95	WT	5°	0°	Full	protrusion	0°
	0.95	Flight	5°	0°	Full	protrusion	0°
	0.95	Flight	5°	10°	Full	protrusion	0°
	0.95	Flight	5°	45°>135°,45°	Full	protrusion	0°
Supersonic	1.80	WT	5°	0°	Full	protrusion	0°
	1.80	Flight	5°	0°	Full	protrusion	0°
	1.80	Flight	5°	10°	Full	protrusion	0°
	1.80	Flight	5°	45°>135°,45°	Full	protrusion	0°
Hypersonic	5.00	Flight	5°	0°	Full	protrusion	0°
	5.00	Flight	5°	10°	Full	protrusion	0°
	5.00	Flight	5°	45°>135°,45°	Full	protrusion	0°

DOI: 10.13009/EUCASS2019-130

The adopted reference axis systems for the calculation of the aerodynamic coefficients are reported in Figure 2 and follows the classical aeronautical convention. In particular for the body axis reference system we have: origin on launcher base; x axis along model centreline, positive towards the nose; y axis normal to x in the horizontal plane, positive right; z axis normal to x and y, positive following right – hand rule. The wind axis reference system is obtained by rotation of the angle of attack around the y_b axis. The moments are positive if counter-clockwise (as in figure) while for the forces we have: $CA=-CX_b$, $CN=-CZ_b$; $CD=-CX_a$, $CL=-CZ_a$, $CS=CY_b=CY_a$.

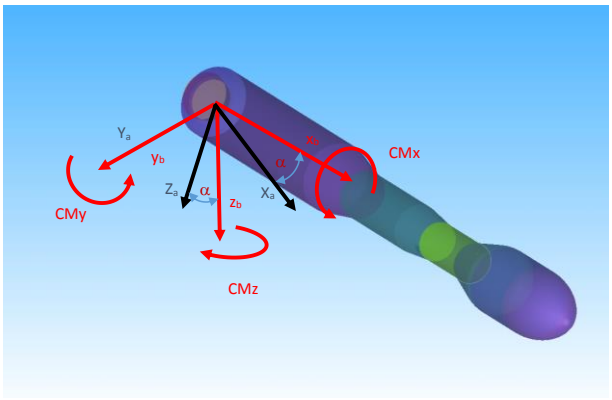

Figure 2: Body and wind reference system.

Several grids have been used in order to perform the present simulations: 4-stage for sub-transonic (M_∞ from 0.5 to 1.2), 4 stage for supersonic (M_∞ from 1.7 to 2.0), clean and 6 degrees canted nozzle, 4-stage for hypersonic (Mach 3.5 – 6.0) and 3-stage for hypersonic (Mach = 4.0 – 7.0). For the 4-stage configuration additional and full-body grids was generated for sub-transonic-supersonic and hypersonic. The Grid characteristics are reported in Table 3.

Table 3: Main characteristics of the Grids

	4Stage sub-trans	**4Stage supersonic**	**4Stage supersonic canted**	**4Stage hyper**	**3Stage hyper**	**4S Prot Sub-trans-super**	**4S Prot hyper**
Levels	3	3	3	3	3		
Cells (million)	13.3	13.3	13.3	4.1	3.5	72	11
Blocks	13	13	13	77	65		

In the following figures, some pictures of the grids are reported.

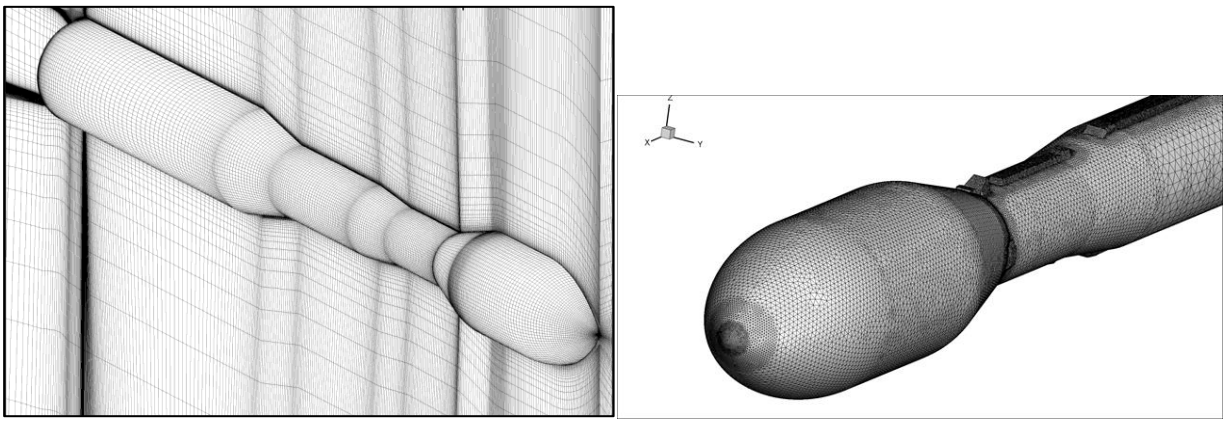

Figure 3: Clean Transonic Grids (left) and Protrusion Hypersonic Grid (right).

The grid sensitivity analysis has been conducted in order to be sure of using a proper number of points. The case of the 4S-hyper configuration at Mach = 5.00, α=5° is depicted in the following Figure 4. Three grid levels have been considered, the lower levels being obtained by halving the amount of cells of the finer grid in each direction. The

DOI: 10.13009/EUCASS2019-130

trend of pitching moment coefficient and centre of pressure (X_{cp}) is reported versus the parameter h that is representative of the average value of the grid dimension: $h= 1/(Cells)^{1/3}$

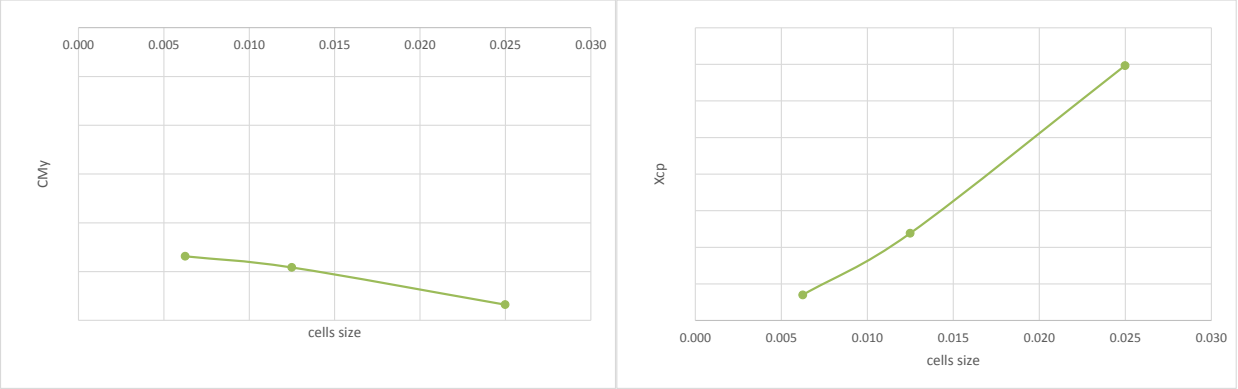

Figure 4: Grid sensitivity analysis for Hypersonic 4-stage configuration: Pitching Moment and Centre of Pressure.

In the following figures some contours plot are reported for Mach 0.95 and 3.50 for clean configuration and M=1.8 for protrusion one. It is interesting to remark, for the Mach=0.95 case, the position of the shock wave in the boat tail region. This required additional investigations in order to foresee a possible buffeting phenomenon due to the fluidynamic instability of this position. No evidence of possible buffeting has anyway been found from this investigation.

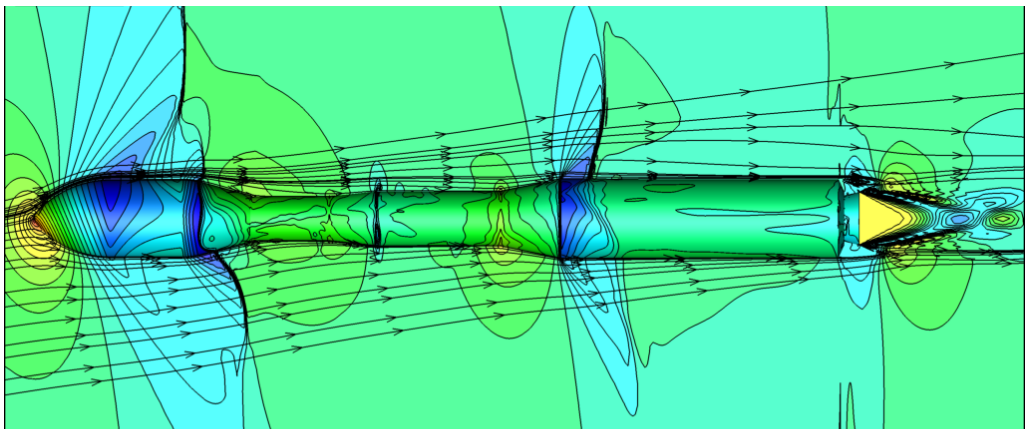

Figure 5: Pressure contours at M=0.95. Clean Configuration.

Figure 6: Pressure contours at Mach 1.80. alpha 5°. Protrusion Configuration.

DOI: 10.13009/EUCASS2019-130

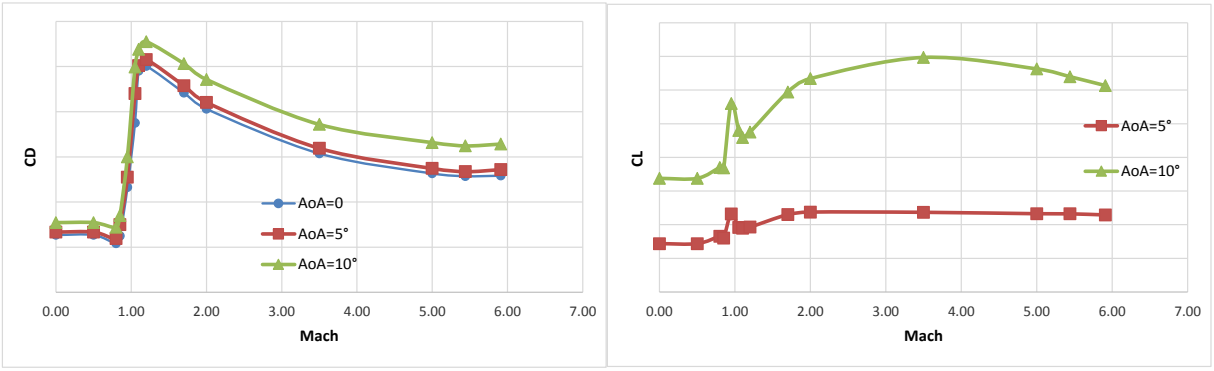

Figure 7: Drag (left) and Lift (right) coefficients vs Mach. Full range of Mach

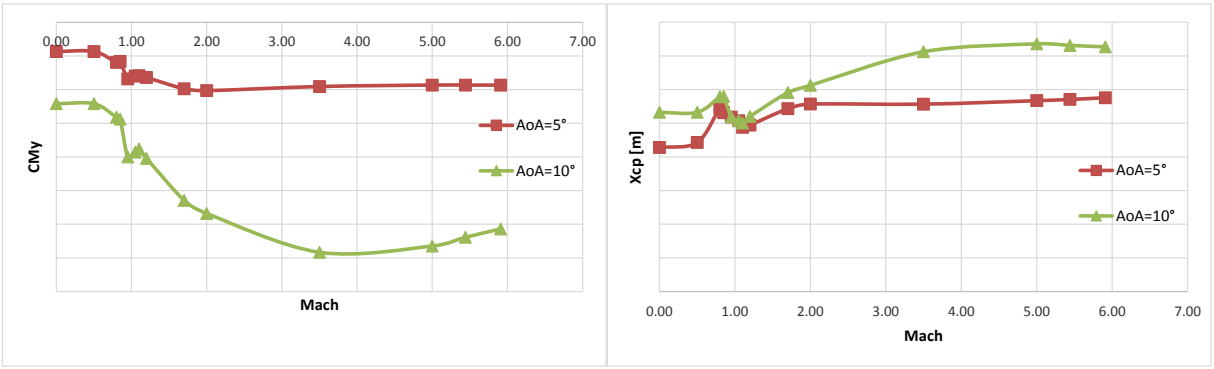

Figure 8: Pitching moment coefficient (left) and Centre of pressure (right) vs Mach. Full range of Mach

The behavior of the main aerodynamic coefficients are reported from Figure 7 to Figure 8. After the transonic range, where typical oscillations can be observed, a flat region arises after Mach 2.0 at the angle of attack of five for lift, pitching moment and centre of pressure. A nonlinear behavior is exhibited versus the angle of attack at all Mach numbers. At ten degrees of angle of attack no flat region is reached up to Mach six for all the coefficients. This behavior can be partially explained by the presence of a non-constant plume of the first stage solid rocket.

5. Experimental activities

The experimental activities have been conducted at the trisonic facility of INCAS institute in Bucharest. It consisted of measurements of forces and pressure distribution, oil flow visualizations, Schlieren visualizations and acoustic characterization. The building of AEDB needs, as specified in a previous section, values of forces (aerodynamic coefficients) and pressure distributions that help the comprehension of flow field structure and can allow the calculation of distributed and lumped coefficients (load distributions). It has to be specified that these last values have been evaluated at the end by means of CFD calculations. Next tables contain the experimental test matrices for measurements of forces and pressures for both clean and protrusions configurations.

Table 4: Experimental Test Matrix. 4 stage Clean Configuration. 52 polars.

Regime	**Mach** [-]	**Reynolds** [-]	**AoA** [deg]	**ϕ (roll)** [deg]	**Conf.**	**# Polars** [deg]
Sub-Transonic	0.50	5.0 10^6	-10°,-5°,0°,5°,10°	-30°, 0°	baseline	2
	0.80	8.0 10^6	-10°->10°, st 1°	0°	baseline	1
	0.85	8.0 10^6	-10°->10°, st 1°	0°	baseline	1
	0.95	2.5 10^6	-2°->10°, st 1°	0°	baseline	1
	0.95	8.0 10^6	-10°->10°, st 1°	-30°->120°, 30°	baseline	6
	1.05	2.5 10^6	-2°->10°, st 1°	0°	baseline	1

DOI: 10.13009/EUCASS2019-130

	1.05	8.0 10^6	-10°->10°, st 1°	Half	baseline	6
	1.10	8.0 10^6	-10°->10°, st 1°	0°	baseline	1
	1.20	2.5 10^6	-2°->10°, st 1°	0°	baseline	1
	1.20	8.0 10^6	-10°->10°, st 1°	-30°->120°, 30°	baseline	6
Supersonic	1.80	2.5 10^6	-2°->10°, st 1°	0°	baseline	1
	1.80	8.0 10^6	-10°->10°, st 1°	-30°->120°, 30°	baseline	6
	2.00	2.5 10^6	-2°->10°, st 1°	0°	baseline	1
	2.00	8.0 10^6	-10°->10°, st 1°	-30°->120°, 30°	baseline	6
	3.00	5.0 10^6	-2°->10°, st 1°	-30°->120°, 30°	baseline	6
	3.50	3.8 10^6	-10°->10°, st 1°	-30°->120°, 30°	baseline	6

Table 5: Experimental Test Matrix. 4 stage Protrusion Configuration. 48 polars.

Regime	**Mach** [-]	**Reynolds** [-]	**AoA** [deg]	**ϕ (roll)** [deg]	**Conf.**	**# Polars** [deg]
Sub-Transonic	0.50	5.0 10^6	-10°,+10°	-75°,-60°,-30°,0°, 10°,45°,90°,135°	protrusion	8
	0.80	8.0 10^6	-10°->10°	-75°,-60°,-30°,0°, 10°,45°,90°,135°	protrusion	8
	0.95	2.5 10^6	-10°->10°	-75°,-60°,-30°,0°, 10°,45°,90°,135°°	protrusion	8
	1.20	8.0 10^6	-10°->10°	-75°,-60°,-30°,0°, 10°,45°,90°,135°	protrusion	8
Supersonic	1.80	8.0 10^6	-10°->10°	-75°,-60°,-30°,0°, 10°,45°,90°,135°	protrusion	8
	3.00	3.0 10^6	-10°->10°	-75°,-60°,-30°,0°, 10°,45°,90°,135°	protrusion	8

6. Extrapolation to Flight Procedure

The extrapolation to flight procedure ([4], [5], [6]) is conducted for a subset of Mach numbers in the sub-transonic and low supersonic range from M=0.50 to M=3.5. This procedure is applied to the clean configuration. The contribution of protrusions will be discussed in a next section.

The main steps of the extrapolation to flight procedure are:

- From CFD: computation of Reynolds effect exploiting the simulations conducted at two angle of attack (2°, 5°) and four Reynolds numbers: two in wind tunnel conditions (WT1, WT2) one intermediate between wind tunnel and flight (INT) and one in flight conditions (FL).
- From CFD: computation of Base/Nozzle contribution (that is not measured in wind tunnels test campaign) exploiting the numerical simulations at AoA=2°, 5° at flight Reynolds number (FL).
- From WT data: building, for each Mach number, of the polars in the range of angle of attack between -10° and 10° (1° of step) by means of polynomial fitting.
- Then: building of the final polars in flight conditions by adding to experimental polars the Reynolds effect and Base/Nozzle contributions.

A symmetrizing (anti-symmetrizing for Lift and Moment) and fitting procedure was undertaken for experimental measurements. This allowed us to get "regular" values of experimental polars.

In Figure 9-(left) we can see the built experimental polars for longitudinal coefficients CMy, CL, CD (dashed lines in figures that are fitting from the cloud of points, also reported) and comparison with CFD data in WT conditions (filled circles). Then, after the adding of CFD contribution (Reynolds effect and base/nozzle part), we can see from

DOI: 10.13009/EUCASS2019-130

the Figure 9-(right) the final (extrapolated to flight) polars (continuous lines) and compared with CFD data in flight conditions (filled circles).

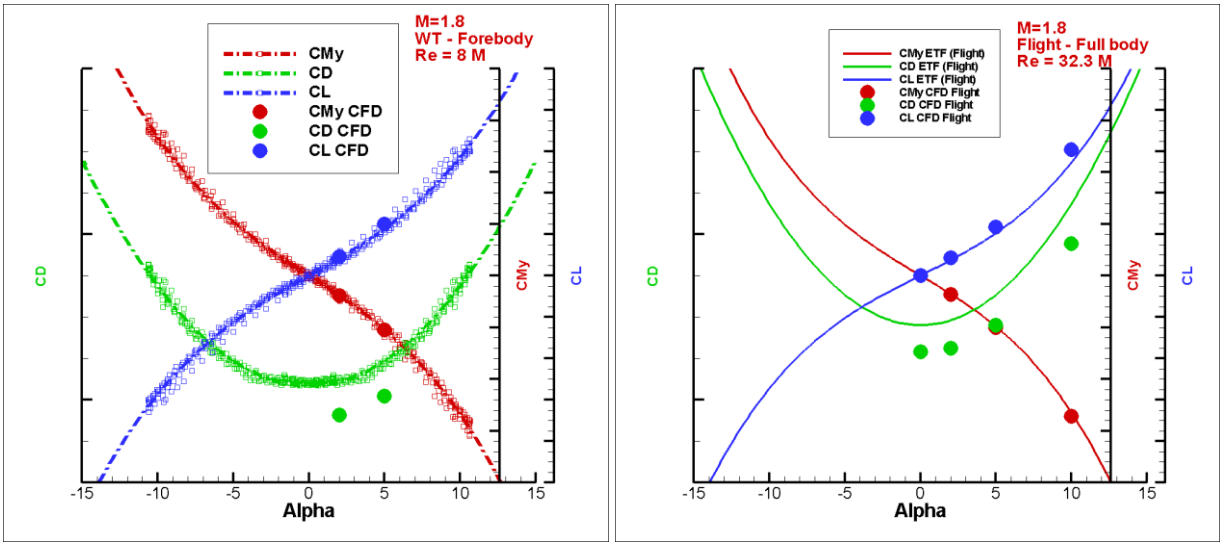

Figure 9: Polars in wind tunnel and extrapolated (flight) conditions. M=1.8.

7. Protrusion Effect

The protrusions effect has been taken into account in three different ways, exploiting several source of data: CFD calculations, former VEGA database and Experimental measurements. The final effect of protrusions takes into account all these affects. In this paper only some numerical results are reported and discussed in order to have idea of the general effect om the clean database. The simulations have been conducted at M=0.95, 1.80, 5.00; AoA=5°. Main results are:

- Delta-CL and Delta-CMy show peaks (in absolute value) at 90° and 270° and minimum values at 0° and 180° (360°) at all analysed Mach numbers. This effect is due the fact that at these values of ϕ the wiring tunnels works as little wings and so giving additional lift.
- Delta-CD shows peaks at 90° and 270° only in hypersonic regime (M=5.00), while in transonic (M=0.95) and supersonic (M=1.80) shows a quasi-constant behaviour and not easy to classify. Unlike the lift coefficient the effect of wiring tunnels, in transonic and supersonic, is not so evident on drag.
- In general the peaks are different at 90° and 270° due to non symmetry of the vehicle with respect to the x-z plane (wiring tunnels of the first stage located at -10° and 190° and not 0° and 180°)
- All the lateral/directional coefficients show a sinusoidal behaviour with peaks (both positive and negative) at phi=45°, 135°, 225° 315° (greek cross) and value near zero at phi=0°, 90°, 180°, 270° (latin cross).
- The value of the rolling moment coefficient (Figure 10) indicate that the flight condition at phi=90° and 270° are of stable equilibrium. In fact in this condition the flight plane (x-y) is of perfect symmetry.
- The flight condition at phi=0° (or phi=180°) is not of equilibrium (due to the non symmetry of first stage wiring tunnels) and in addition (in case of a null rolling moment as in VEGA 2003) is a not stable position. The rolling moment tends to rotate the vehicle towards the stable position at phi=90° or phi=270° (-90°). In any case the value of rolling moment at phi=0° are very small and so easy to manage by the control system.

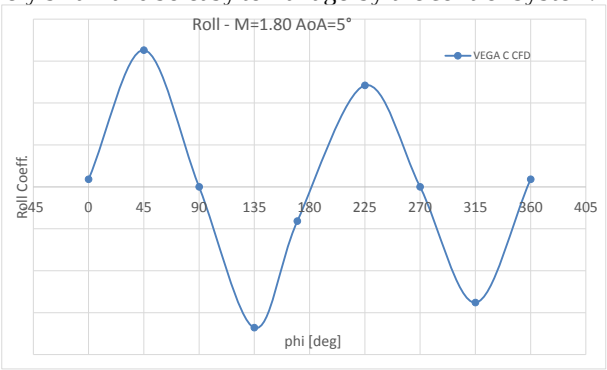

Figure 10: Numerical protrusion effect on roll coefficient at M=1.80, AoA=5°. Flight condition.

DOI: 10.13009/EUCASS2019-130

8. Confidence Level Evaluation

The confidence level is a summation of uncertainty and dispersion. This concept is applicable for both experimental and computational values. The experimental uncertainty is linked to direct measurements (balance) and the dispersion is linked to the repeatability of the same measurements and to additional dispersions due to the differences between the model/model-settings and the real flight conditions. Analogously the numerical uncertainty is due to the grid sensitivity and flow modeling (f. e. turbulence modeling) and the dispersion concerns with the difference between CAD model/run settings and the real world. This last term is taken into account for both experiments and CFD with a suitable factor. The final confidence level is a summation of the experimental contribution (balance and repeatability) and numerical contribution (grid and modeling).
The centre of pressure is a derivative quantity of Pitching Moment and Normal Force and is strictly correlated to them:

$$X_{cp} = -\frac{C_{My}}{C_N} * Lref$$

Once the uncertainties for CMy and CN have been obtained, the following formula is used ([11]):

$$U_{X_{cp}} = \sqrt{{U_{C_{My}}}^2 + {U_{C_N}}^2 - 2 * Corr * U_{C_{My}} * U_{C_N}}$$

Where in the formula the values have to be considered as relative uncertainties and Corr is the correlation between CMy and CN.

$$Corr. = \frac{Covariance\,(C_N, C_{My})}{\sigma_{C_N} * \sigma_{C_{My}}}$$

In general

$$Covariance\,(x,y) = \frac{1}{N}\sum (x_i - \overline{x}) * (y_i - \overline{y})$$

$$\overline{x} = \frac{1}{N}\sum x_i \quad ; \quad \overline{y} = \frac{1}{N}\sum y_i$$

$$\sigma(x) = \sqrt{Variance\,(x)} = \sqrt{\frac{1}{N}\sum (x_i - \overline{x})^2}$$

A value of 0.9 is used and is based on available data of VEGA C repeatability measurements of wind tunnel. The formula is a direct consequence of the propagation error theory. The correlation is a non-dimensional value that ranges from zero (no correlation and higher value of uncertainty) to one (full correlation and lower value of uncertainty). From the above formula we can see that in the particular case of equal values of uncertainties for CMy and CN and full correlation (corr = 1) we can have a null uncertainty for Xcp.
In the next figure is showed, as example, the total uncertainty of lift coefficient at M=1.8.

DOI: 10.13009/EUCASS2019-130

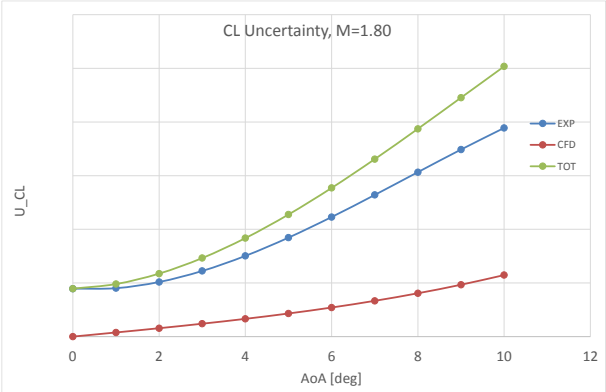

Figure 11: Total Lift Coefficient Uncertainty. M=1.80.

9. Final Aerodatabase

The final aero-database is obtained by adding to the clean values the protrusions effect evaluated in the previous section. In Figure 12, as example, is reported the Lift coefficient at M=1.80. The confidence level bar is also plotted together with the CFD values as comparison. It is worthwhile to note as the CFD values are included in the confidence level bar (error bar).

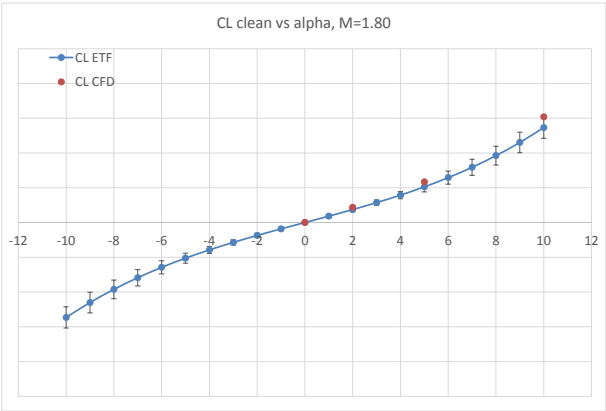

Figure 12: Lift Coefficient with confidence level bar. M=1.80.

A good comparison between numerical results and experimental measurements can be found also in the next figures for what concerns the pressure distributions. We can remark as at m=0.95 the shock position at the end of boat tail perfectly compares (Figure 13).

DOI: 10.13009/EUCASS2019-130

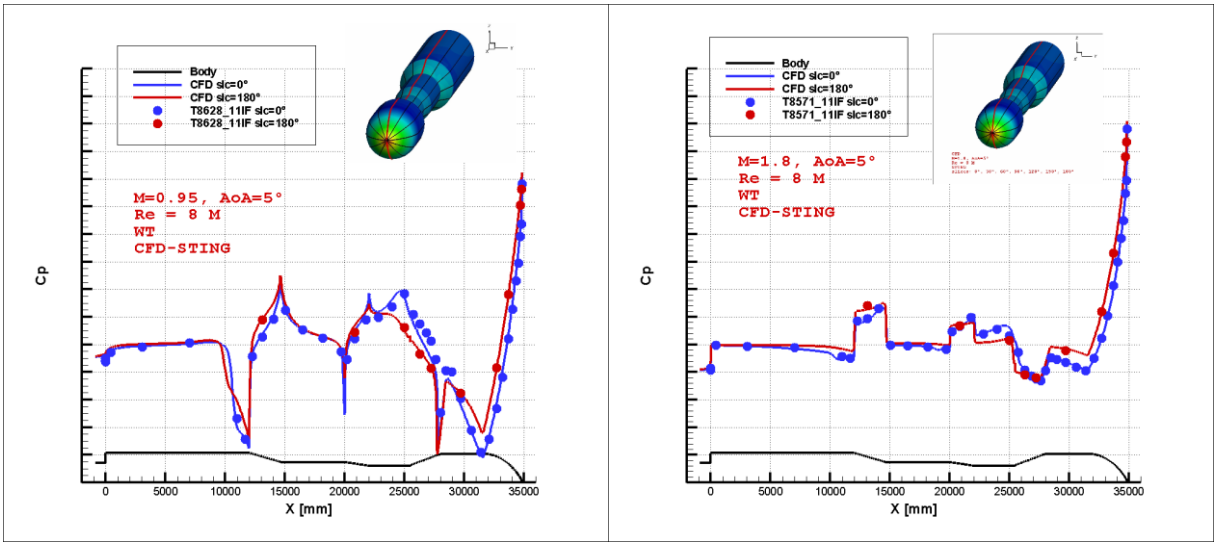

Figure 13: EXP vs CFD Cp distribution. M=0.95 (left), M=1.80 (right).

A qualitatively comparison of Experimental (oil flow) and CFD flow patterns are reported and commented at the end of this paper for M=0.95, 1.80.

M=0.95, AoA=5°

The experimental reattachment occurs about 32mm downstream the boat tail step whereas the CFD results indicates an anticipate reattachment on the upper side with respect to the lower side. The model side view pictures shows a coalescence of the streamlines indicating the formation of two longitudinal vortices on the sides of the launcher growing up on the lower part of the model immediately after the reattachment regions.

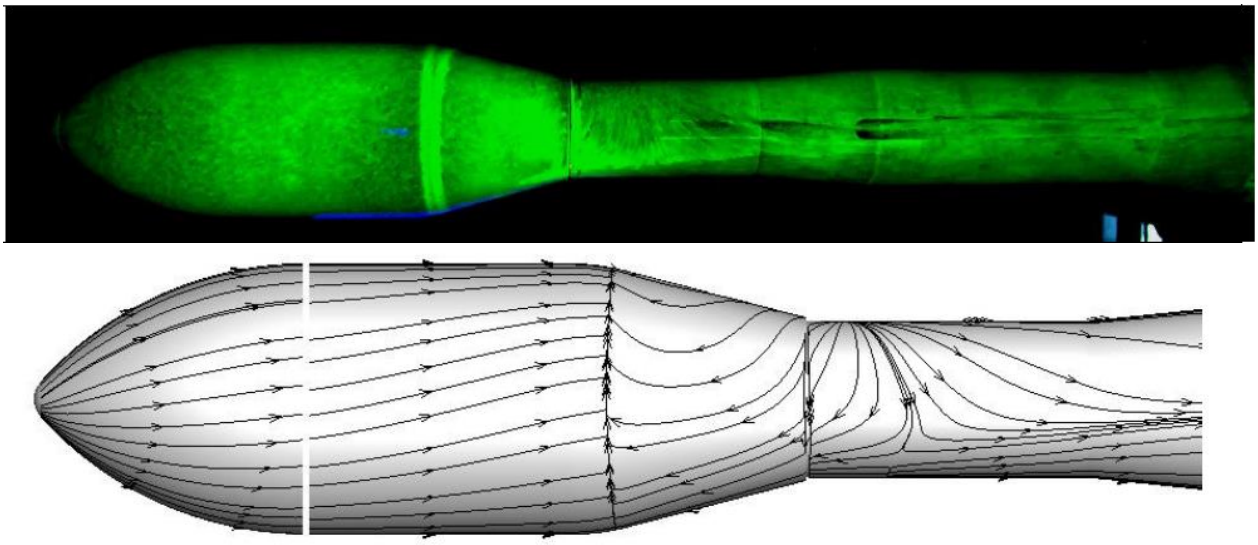

M=1.80, AoA=5°

On the model upper part, the flow separation occurs at distance of x=26.5mm from the end of the boat tail, on the lateral side the flow separation is slightly anticipate at x=27mm and on the lower side the flow separation occurs just a couple of millimetre before the end of the boat tail. The different flow velocity from the upper and lower side induce a swirl velocity that induces the formation of a longitudinal vortex on each side of the launcher. The CFD data obtained at Reynolds of 2.2 million, present similar characteristics. The CFD results depict the flow separation and the presence of the lateral vortices

DOI: 10.13009/EUCASS2019-130

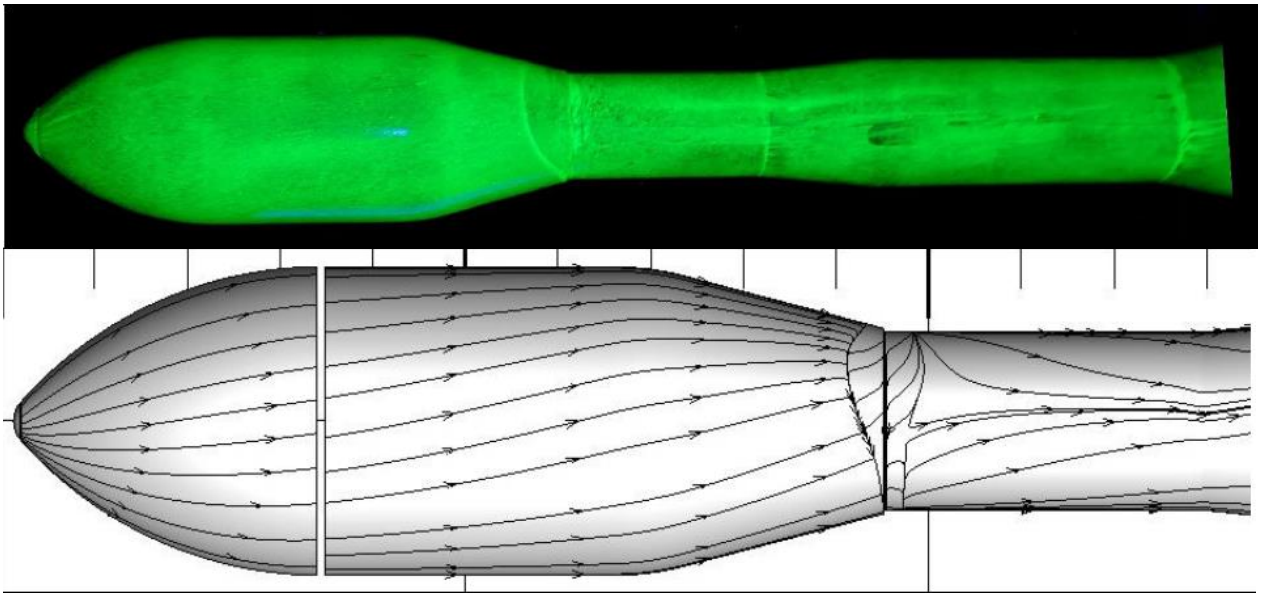

10. Conclusions

In this paper the procedure for the building of the final aero-database of VEGA C Launcher is reported. This procedure is based on clean and protrusion WT data, clean and protrusion CFD computations and on the former VEGA protrusions effect. A confidence level is also provided based on the same base of data.
In particular in this paper is reported:

- The general approach for the ADB building
- The procedure of extrapolation to flight based on CFD simulations performed at several Reynolds number and angles of attack.
- The protrusion effect evaluation
- The confidence level evaluation.

A fitting of clean experimental data is used in order to overcome the scattering of data and some non-symmetrical behaviors.
The final values of the aerodynamic coefficients at flight conditions (ETF) are obtained as a summation of the experimental forebody values (corrected for the Reynolds effect as evaluated by CFD) and the base/nozzle contribution from CFD simulations.
The comparison of ETF and CFD values shows a good behavior for what concerns the trend of global coefficients versus the angle of attack. A comparison of experimental and numerical pressure coefficients distributions at the wind tunnel conditions is also reported together with the flow patterns of both experimental oil flow visualization and CFD wall skin friction lines.

References

[1] Nicolì A, Imperatore B, Fauci R and Pizzicaroli A, 2006 Wind Tunnel Test Campaign of the VEGA Launcher. 44th AIAA Aerospace Sciences Meeting and Exhibit, Reno, Nevada, January 9-12.

[2] Nicolì A, Imperatore B, Marini M, Catalano P, Pizzicaroli A and Perego D, 2006 Ground-to-Flight Extrapolation of the Aerodynamic Coefficients of the VEGA Launcher. 25th AIAA Aerodynamic Measurement Technology and Ground Testing Conference, San Francisco, California, June 5-8.

[3] Catalano P, Marini M, Nicolì A, Pizzicaroli A, 2007 CFD Contribution to the Aerodynamic Data Set of the Vega Launcher. Journal of Spacecraft and Rockets 44: 42-51.

[4] Roncioni P., G. C Rufolo, M. Marini. 2006 AN EXTRAPOLATION TO-FLIGHT METHODOLOGY FOR WIND TUNNEL MEASUREMENTS APPLIED TO THE PRORA-USV FTB1 VEHICLE. *57th International Astronautical Congress, Valencia, Spain; October.*

[5] Roncioni P., G. C. Rufolo, M. Marini, S. Borrelli. 2009. CFD rebuilding of USV-DTFT1 vehicle in-flight experiment. *Acta Astronautica 04/2010; 66(7-8-66):1201-1219. DOI:10.1016/j.actaastro.2009.10.015.*

[6] Roncioni P., G. Ranuzzi, M. Marini, E. Cosson, T. Walloschek. 2011. Experimental and Numerical Investigation of Aerothermal Characteristics of Hypersonic Intermediate Experimental Vehicle. *Journal of Spacecraft and Rockets 04/2011; 48:291-302. DOI:10.2514/1.48331.*

DOI: 10.13009/EUCASS2019-130

[7] Boerstoel, J. W., J. M. Jacobs, J. W., Kassies, A., Amendola, A., Tognaccini, R., Vitagliano, P. L. 1989. "Design and testing of a multiblock grid-generation procedurefor aircraft design and research", *AGARD CP 464, No 9, pp. 1-16*.

[8] Boerstoel, J. W., S. P. Spekreijse, P. L. Vitagliano. 1992. "Design of a system of codes for industrial calculations of flows around aircraft and other complex aerodynamic configurations", *AIAA-1992-2619-CP, pp. 207-229*.

[9] Catalano, P., M. Amato. 2003. "An evaluation of RANS turbulence modelling for aerodynamics applications", *Aerospace Science and Technology, October, pp. 493-509*.

[10] Jameson, A. 1991. "Time-Dependent Calculations Using Multigrid, with Application to Unsteady Flows past Airfoils and Wings", *in AIAA paper 91-1596 proceedings of the 10th AIAA Computational Fluid Dynamics conference in Honolulu, HI, USA, 1991, AIAA*.

[11] Clifford, A. A. 1973, "Multivariate error analysis: a handbook of error propagation and calculation in many-parameter systems", John Wiley & Sons.

[12] Kok, J. C. 2000. "Resolving the dependence on free-stream values for the k-ω turbulence model", *AIAA J., Vol 38, No 7, 2000, pp. 1292-1295*.

[13] Marongiu, C., P. Catalano, M. Amato, G. Iaccarino. 2004. "U-ZEN: a computational tool solving U-RANS equations for industrial unsteady applications", *in AIAA paper 2004-2345 proceedings of the 34th AIAA Fluid Dynamics conference in Portland, OR, USA, 2004, AIAA*.

[14] Marongiu, C., A. Panizza, P. L. Vitagliano. 2007. "A moving grid method for unsteady flow computations", *18th AIAA Computational Fluid Dynamics Conference, Miami, FL, USA, 2007, AIAA 2007-4470*.

[15] Kok, J.C., M. Amato, S. Bosse, A. Kassies. 1993. "Numerical design of ENSOLV; a code for the numerical simulation of 3D flows using the Thin Layer Navier-Stokes and Euler equations" *CIRA-DLC-EST-TR-265, NLR CR 93152 L*

[16] Ranuzzi G., D. Cardillo, M. Invigorito. 2015. "Numerical Investigation of a N2O-Paraffin Hybrid Rocket Engine Combusting Flowfield", *6th European Conference For Aeronautics And Space Sciences, July*.

[17] Grasso F., Falconi D. 1993. "High-Speed Turbulence Modeling of Shock-Wave/Boundary-Layer Interaction", *AIAA Journal, Vol. 31, No 7, July*.

[18] Thompson, J.F., Z.U.A.Warsi, C.W Mastin. 1985. "Numerical grid generation. Foundations and applications." *North Holland*.